Novel Class of Antibiotics Disassembles the Lipopolysaccharide Transport Bridge

Oliver Zerbe (oliver.zerbe@chem.uzh.ch)
University of Zurich https://orcid.org/0000-0003-0475-438X
Matthias Schuster
University of Zurich
Emile Brabet
Spexis AG
Kathryn Oi
University of Zurich
Nicolas Desjonquères
Spexisbio
Kerstin Moehle
University of Zurich
Karen Poupon
Spexisbio/Bright Peak Therapeutics
Sopie Hell
Spexisbio/Bright Peak Therapeutics
Stéphane Gable
Spexisbio/Bright Peak Therapeutics
Virginie Rithié
Spexisbio/Bright Peak Therapeutics
Séverine Dillinger
Spexisbio
Peter Zbinden
Spexis AG
Anatol Luther
Spexisbio/Bachem
Claudia Li
Spexisbio
Sarah Stiegeler
Spexisbio/Trinity College
Carolin D'Arco
Spexisbio
Hans Locher

Spexisbio
Tobias Remus
Spexisbio
Selena DiMaio
Spexisbio
Paola Motta
Spexisbio/Vifor Pharma
Achim Wach
Spexisbio
Françoise Jung
Spexis AG https://orcid.org/0000-0003-2791-2934
Gregory Upert
Spexis AG
Daniel Obrecht
Spexis AG
Mohammed Benghezal
Spexisbio

Biological Sciences - Article

Keywords:

Posted Date: April 11th, 2022

DOI: https://doi.org/10.21203/rs.3.rs-1525565/v1

Novel Class of Antibiotics Disassembles the Lipopolysaccharide Transport Bridge

Matthias Schuster[1,#], Emile Brabet[2,#], Kathryn K. Oi[1,#], Nicolas Desjonquères[2], Kerstin Moehle[1], Karen Le Poupon[2,3], Sophie Hell[2,3], Stéphane Gable[2,3], Virginie Rithié[2,3], Séverine Dillinger[2], Peter Zbinden[2], Anatol Luther[2,4], Claudia Li[2], Sarah Stiegeler[2,5], Carolin D'Arco[2], Hans Locher[2], Tobias Remus[2], Selena DiMaio[2], Paola Motta[2,6], Achim Wach[2], Françoise Jung[2], Grégory Upert[2,3], Daniel Obrecht[2]*, Mohammed Benghezal[2*], Oliver Zerbe[1*]

[1] University of Zurich, Winterthurerstrasse 190, CH-8057 Zurich, Switzerland
[2] Spexis AG, Hegenheimermattweg 125, CH-4112 Allschwil, Switzerland
[3] current address: Bright Peak Therapeutics, Basel, Switzerland
[4] current address: Bachem AG, Bubendorf, Switzerland
[5] current address: Trinity College Dublin, Ireland
[6] current address: Vifor Pharma, Zurich, Switzerland
[#] contributed equally
[*]corresponding authors: daniel.obrecht@spexisbio.com; mbenghezal@gmail.com; oliver.zerbe@chem.uzh.ch

Prof. Oliver Zerbe
Department of Chemistry
University of Zurich
Winterthurerstrasse 190
CH-8057 Zurich, Switzerland
phone: +41-44-635 42 63
email: oliver.zerbe@chem.uzh.ch

Dr. Daniel Obrecht/ Dr. Mohammed Benghezal
Spexis AG
Hegenheimermattweg125,
CH-4123Allschwil, Switzerland
phone: +41-61-567 16 00
email: daniel.obrecht@spexisbio.com; mohammed.benghezal@spexibio.com

Summary

The rapid rise of multi-resistant bacteria poses a significant threat to our health system. The development of drugs against novel targets is urgently needed to replenish the clinical arsenal with effective antibiotics. The naturally occurring peptide thanatin kills Gram-negative bacteria by targeting the periplasmic protein bridge, in particular the lipopolysaccharide transport protein A (LptA).

Using the thanatin scaffold together with phenotypic medicinal chemistry and a target-focused approach, we developed potent antimicrobial macrocyclic peptides with drug-like properties that exhibited low frequencies for development of resistance both *in vitro* and *in vivo*. Binding affinities to *Escherichia coli* LptA of the thanatin analogs correlated well with minimal inhibitory concentrations for both parent and thanatin-resistant *E. coli* strains. Mode of action studies revealed that the antimicrobial activity of the antibiotics involves the specific disruption of the periplasmic Lpt protein bridge. Our studies validate the Lpt protein bridge as a novel target for macrocyclic peptide antibiotics that can avoid current mechanisms of drug resistance. The peptides warrant further preclinical and clinical studies addressing WHO priority 1 carbapenem-resistant Enterobacteriaceae, in particular for *Klebsiella pneumoniae* lung infections.

Introduction

In 2019, 5 million deaths due to antimicrobial resistant (AMR) organisms were reported worldwide[1]. Of those, 1.3 million were from the WHO classified priority 1 ESKAPE pathogens (*Enterococcus faecium*, *Staphylococcus aureus*, *Klebsiella pneumoniae*, *Acinetobacter baumannii*, *Pseudomonas aeruginosa*, and *Enterobacter spp*). Thus, there is a critical and growing need to replenish the arsenal of standard-of-care antibiotics to bring new solutions to AMR bacterial infections[2,3], in particular against carbapenem-resistant Enterobacteriaceae (CRE)[3] that cause difficult-to-treat nosocomial infections [4].

One way of reducing the threat from AMR organisms is the development of drugs against novel targets. Essential proteins located at the outer membrane of Gram-negative bacteria represent such an untapped target source. Recently, naturally occurring peptides were proposed to interfere with the function of proteins involved in the transport of lipopolysaccharides (LPS) from the inner to the outer membrane or the β-barrel assembly machinery (BAM)[5-8]. LPS transport is accomplished by a system of seven proteins, called Lpt proteins A-G (Fig. 1)[9-11]. The periplasmic protein bridge is composed of LptA homooligomers anchored to LptD and LptC at the outer and inner membranes, respectively. Dysregulation of lipid A biosynthesis and LPS transport results in lethal LPS accumulation at the inner membrane[5,12-17].

Thanatin, a 21-amino acid hairpin peptide isolated from the gut of the hemipteran insect *Podisus maculiventris*[18], binds to both LptA and LptD[16,19]. We hypothesized that thanatin acts as a competitive inhibitor of protein-protein interactions of the Lpt bridge (Fig. 1) thereby inhibiting LPS transport across the periplasm. Of note, thanatin is not a suitable drug candidate for further development due to poor druglike properties and rapid emergence of resistance[16].

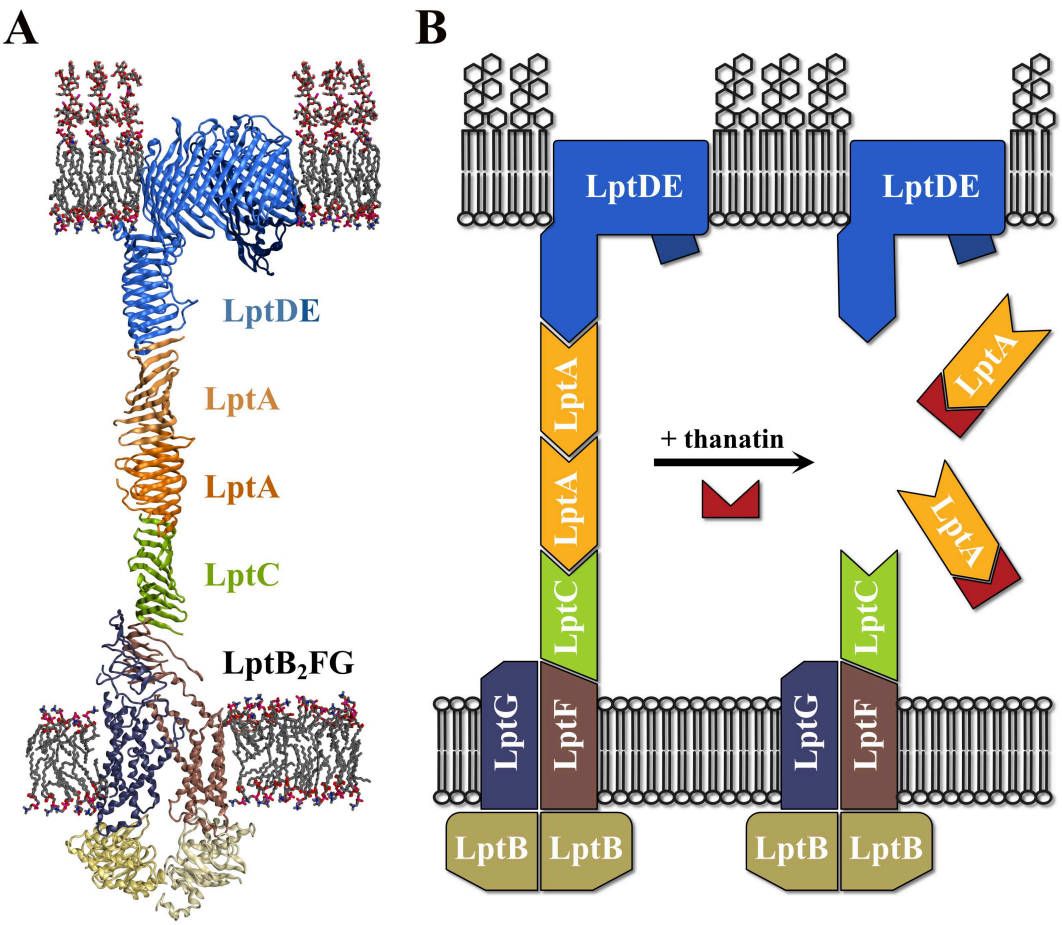

Fig. 1: **A** Structural model of the Lpt bridge across the periplasm of Gram-negative bacteria, and **B** the postulated mode of action based on this work, in which thanatin interrupts the bridge integrity by complexing LptA. Note that only 2 LptA proteins are depicted although the actual number might vary.

Inspired by thanatin, we describe the identification of novel peptide drug candidates with potent antimicrobial activity *in vitro* and in mouse infection models against CRE, favorable absorption, distribution, metabolism and excretion (ADME) and safety profile. Importantly, these peptides display low propensity for resistance development. We show that these peptides bind in the low nanomolar range to LptA, and provide direct biophysical evidence that they disassemble the Lpt protein bridge and thereby block LPS translocation across the periplasm.

Drug discovery

Initial hit compounds were obtained by truncating the N-terminus of thanatin. The 19-mer peptides **1** and **2** (Fig. 2) showed an increase in antimicrobial activity against the parent strains. In contrast, truncations at the C-terminus reduced the activity. Subsequent systematic replacement of residues with natural or unnatural amino acids at positions 11 (Cys to L-Penicillamine (Pen)) and 16 (Gly to (D)-2,4-Diaminobutyric acid (DDab)) were identified as key changes to increase peptide stability in blood plasma, as observed for **2** (Tab. S4A). Furthermore, incorporation of a cationic amino acid with a short side chain, 2,4-diaminobutyric acid (Dab), at positions 14 and 19, enhanced potency and mitigated toxicity. When tested against the thanatin-resistant *E. coli* ATCC 25922 strain harboring the LptA^{Q62L} mutation[16], these peptides displayed both high antimicrobial activity and low resistance susceptibility.

A

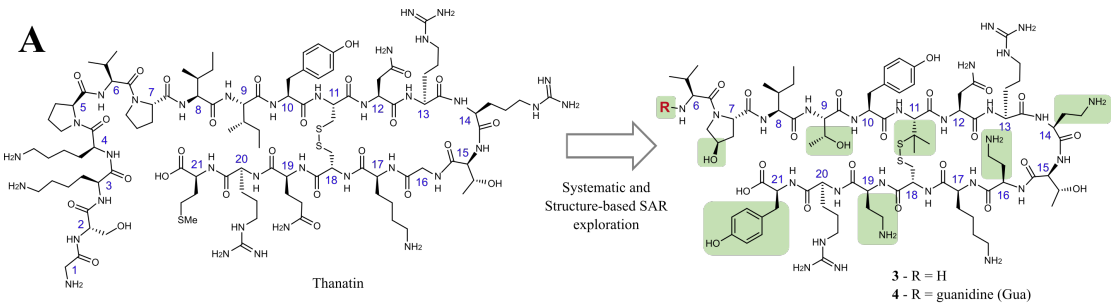

B

Peptide	Position 1	2	3	4	5	6	7	8	9	10	11	12	13	14	15	16	17	18	19	20	21
Thanatin	G	S	K	K	P	V	P	I	I	Y	C	N	R	R	T	G	K	C	Q	R	M
1			K	K	P	V	P	I	I	Y	C	N	R	R	T	G	K	C	Dab	R	Nle
2			K	K	P	V	P	I	I	Y	Pen	N	R	Dab	T	DDab	K	C	Dab	R	Y
3						V	Hyp	I	T	Y	Pen	N	R	Dab	T	DDab	K	C	Dab	R	Y
4					Gua	V	Hyp	I	T	Y	Pen	N	R	Dab	T	DDab	K	C	Dab	R	Y
5						V	Hyp	I	I	Y	Pen	N	R	Dab	T	DDab	K	C	Dab	Dab	Y

Fig. 2: Thanatin and new analogues. A, Chemical structures of thanatin and of the new antibiotic peptide analogues **3** and **4**. Structural modifications implemented during the medicinal chemistry optimization are highlighted in green. **B,** Amino acid sequences (one letter code) of the described peptides. Abbreviations: Nle, Norleucine; Pen, L-Penicillamine; Dab, L-2,3-Diaminobutyric acid; DDab, D-2,3-Diaminobutyric acid; Hyp, trans-4-Hydroxy-L-proline; Gua, guanidine.

Further modifications, guided by the structural data obtained by NMR (*vide infra*), resulted in the 16-mer analogues **3**, **4** and **5** (Fig. 2) that displayed *in vitro* activities comparable to **2**, with **5** exhibiting the highest antimicrobial activity against the LptA^{Q62L} resistant mutant (Tab. 1). We suspected that the frequency of resistance is

lower for peptides with highest activity against resistant strains. Hence, we focused on compounds **4** and **5** in our subsequent studies.

Tab. 1: MIC and K_i values of the compounds against different strains and mutants

	***E. coli* ATCC 25922**				***K. pneumoniae* NCTC 13443**			
	Wild-Type		**Q62L mutant**		**Wild-Type**		**Q62L mutant**	
	MIC*	**Ki****	**MIC***	**Ki****	**MIC***	**Ki****	**MIC***	**Ki****
Thanatin	2	2.7 ± 0.2	>8	33.8 ± 5.6	8	1.8 ± 0.1	>8	38.9 ± 7.9
1	0.06	1.1 ± 0.1	>8	20.5 ± 6.0	0.5	0.9 ± 0.1	>8	18.2 ± 5.8
2	0.03	2.1 ± 0.1	2	13.1 ± 4.2	0.5	1.5 ± 0.1	>8	14.5 ± 4.1
3	0.13	2.8 ± 0.2	1	9.9 ± 1.7	2	2.2 ± 0.1	>8	25.3 ± 7.7
4	0.06	1.9 ± 0.1	2	17.2 ± 3.1	0.5	2.0 ± 0.1	>8	16.1 ± 3.4
5	0.06	3.1 ± 0.2	0.25	9.4 ± 1.5	1	1.8 ± 0.1	4	22.5 ± 6.1

**MIC values (in mg L^{-1}) were determined using the CLSI method.*
***Ki values (in nM) were measured by fluorescence polarization. Error range indicate the 95% confidence interval of the fit.*

Both the lead compound **4** and thanatin displayed a narrow activity spectrum encompassing Enterobacteriaceae, except for Yersiniaceae and Morganellaceae (Tab. S5). Compared to thanatin, all compounds showed markedly lower MIC values. High primary sequence conservation of LptA within Enterobacteriaceae correlated well with the antibacterial activities of the peptides. Bacteria with LptA sequence identity < 70% to *E. coli* were largely insensitive to compound **4** (Tab. S5).

Biological profiling

In vitro activity against a panel of 121 Enterobacteriaceae including CRE, multidrug-resistant (MDR) and extensively drug-resistant (XDR) isolates revealed MIC_{90} values of 8 mg/L, 1 mg/L and 0.5 mg/L for thanatin, **3** and **4** respectively (Tab. S6).
All compounds displayed similar plasma protein binding and no haemolytic activity against red blood cells. Importantly, stabilization of the disulfide bridge with the Pen-11 (Fig. 2) significantly improved *in vitro* stability in plasma and increased *in vivo* plasma exposure resulting in improved pharmacokinetics (PK) in mice (Tab. S4B).
Cytotoxicity towards HeLa cells decreased with the reduction of the scaffold length (**1** and **5**) (Tab. S4A).
Intravenous (IV) administration of compound **4**, twice a day (q12h), was tolerated up to a maximum tolerated dose of 30 mg/kg/day in mice. Safety assessment in a 7-day

repeated dosing safety study in mice after IV administration (q12h) showed that compounds **3** and **4** were well tolerated without any findings (Tab. S4B).

Development of resistance of thanatin was observed after 1 day of passaging in both *E. coli* and *K. pneumoniae*, characterized by a spontaneous frequency of resistance of $1.2x10^{-6}$ for *E. coli* at 4xMIC. New analogues delayed resistance development in *E. coli* and *K. pneumoniae* to later passages at 4xMIC, after 3 to 6 days or 3 to >10 days, respectively (Fig. S8), with spontaneous frequencies of resistance of $8.6x10^{-9}$, $1.3x10^{-7}$ and $<3.7x10^{-9}$, in *E. coli* and $2.9x10^{-7}$, $3.8x10^{-8}$ and $<3.1x10^{-9}$ in *K. pneumoniae* for compounds **3, 4** and **5**, respectively (Tab. S7).

Whole genome sequencing of spontaneous resistant mutants revealed that mutations within LptA were the most recurrent (Tab. S8). Among the LptA mutations, Q62L was the prominent mutation conferring moderate-to-high levels of resistance while other LptA mutations resulted in only slight increases in MIC values (Tab. S9**)**. No mutation was identified in the LPS transport bridge anchors LptC and LptD. Further mutations resulting in slight increases of MIC values were observed in either lipid A biosynthesis and regulation, in peptide transporters, metabolism, protein N-glycosylation or non-annotated open reading frames.

***In vivo* activity**

In vitro activity translated *in vivo* with potent efficacy in several neutropenic mouse models of peritonitis (Fig S7A), thigh and lung infections (Fig. 3). A dose response study of **4** in the *K. pneumoniae* AR-BANK#0160 lung infection model established an ED_{50} of 3.4 mg/kg/day q12h, confirming potent activity against CRE (Fig. S7C).

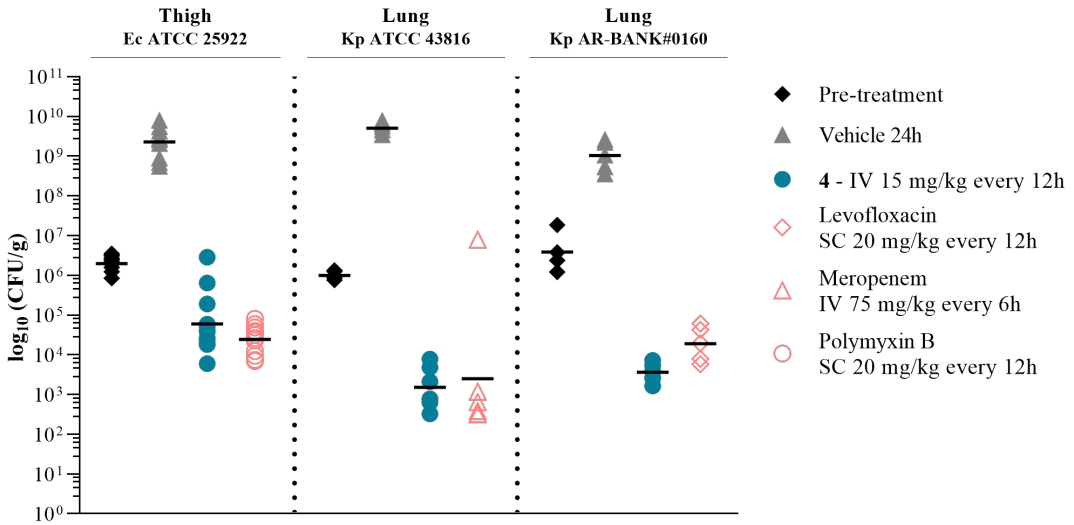

Fig. 3: *in vivo* efficacy of peptide 4. Peptide **4** activity against *E. coli* ATCC 25922 in mouse neutropenic thigh, *K. pneumoniae* AR-BANK#0160 and *K. pneumoniae* ATCC 43816 in mouse neutropenic lung models. CFU counts 24h post first administration of compound **4** (blue), vehicle only (grey), and standard of care (red) are compared. The geometric mean value of each group is depicted as a black dash.

Mode-of-action studies

Structural biology reveals the molecular determinants of binding affinity

To investigate the mode-of-action of these peptides, we studied their complexes with the terminally truncated monomeric version of LptA (LptAm)[20] by NMR. Chemical shift mapping indicated very similar binding modes to LptA for **4** and **5** when compared to thanatin (Fig. S18). The solution structure of the complex reveals that peptide **4** binds to LptAm of *E. coli* and *K. pneumoniae* in an almost identical fashion such that the N-terminal strand of the β-hairpin (P7'-N12') docks in a parallel orientation onto the first N-terminal β-strand (P35-S40) of the β-jellyroll of LptAm.

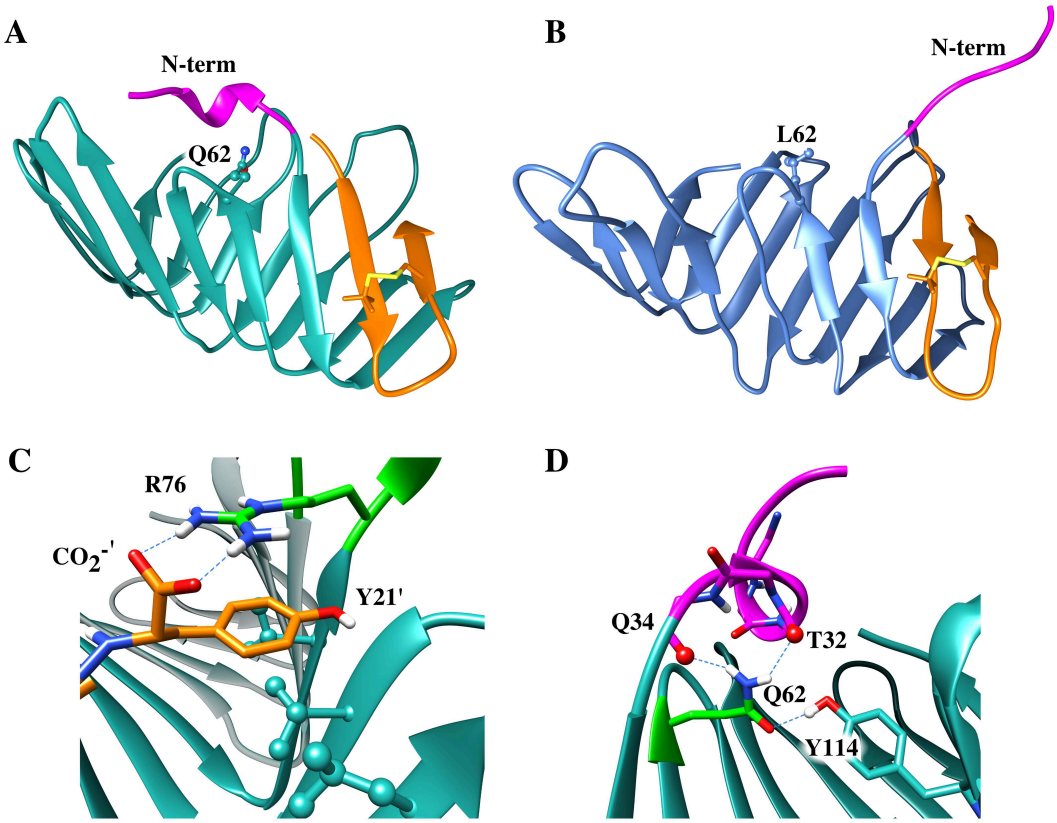

Fig. 4: Structures of the *E. coli* LptAm-**4** complex (**A**) and the LptAm^{Q62L}-**4** complex (**B**). The protein backbone is depicted in green, the peptide in orange. The N-terminal region is displayed in magenta. (**C**,**D**) Stabilizing interactions of the C-terminus of the peptide with LptAm (**C**) and of Q62 with the N-terminal helix (**D**). Peptide residues in (**C**) are highlighted with an apostrophe. For a comparison of the LptAm complexes from *E. coli* and *K. pneumoniae* with **4** see Fig. S20.

The binding interface of LptAm is comprised of the first β-strand between P35-S40, forming a hydrophobic network involving I36, I38, L45, V52, F54, V74, which interact with I8', Y10' and Y21' of peptide **4** such that multiple van der Waals contacts and π-π stacking interactions stabilize the complex. In addition, a salt bridge between the guanidinium group of R76 of LptAm and the carboxy terminus of **4** is formed. The latter interaction is additionally stabilized by a cation-π interaction between R76 of LptAm and Y21' of **4** (Fig. 4B). Further information on side-chain interactions was derived from an MD simulation (Fig. S23). The simulation reveals that R13' forms hydrogen bonds to the carbonyl atom of N57 and a salt bridge with the carboxylate group of D41 (Fig. S19). Interestingly, the side chain of R13' fills a shallow pocket formed by LptA that is occupied in an analogous way by R159 at the interface of the LptA-LptA dimer (Fig S19). In addition, the N-terminal short helix (D31-Q34) is stabilized by a stable hydrogen bonding network that helps to anchor the helix onto the β-jellyroll and contributes to the stability of the folded protein (Fig 4D).

Interestingly, the N-terminal helix is absent in the thanatin-resistant mutant LptAm^{Q62L}. Crucial structural features of the LptAm-**4** interface such as the interaction between the protein and peptide β-strands, the π-π stacking between F54 and Y10', and the salt bridge between R13' and N57, are retained in the LptAm^{Q62L}-**4** complex. However, the missing stabilizing interactions of the N-terminal helix with the β-jellyroll in the mutant complex (Fig. 4C) resulted in an increased overall RMSD (1.1 Å for LptAm versus 1.6 Å for LptAm^{Q62L}). In agreement, RMSD fluctuations of residues V29-Q34 increased by a factor of 2-4 during MD simulations. The reduced number of intermolecular contacts (Tab. S13) coincides with the reduced binding affinity of **4** to LptAm^{Q62L} (K_i = 17.2 nM for LptAm^{Q62L} versus K_i = 1.9 nM for LptAm).

Interactions of Lpt proteins in the periplasmic bridge

In the periplasmic bridge, the N-terminal β-strand of LptA binds in a head-to-tail fashion to the C-terminus of another LptA monomer, the C-terminus of LptC and the N-terminus of LptD (Fig. 1). To understand how peptide antibiotics compete with these interactions, we determined affinities of LptA to peptides **2**-**5** and to LptA and LptC. To unambiguously determine affinities of the LptA-LptA interaction, two monomeric LptA mutants were used, a known C-terminal truncation[20], referred to as LptAm, and a second mutant, mLptA, with 3 mutations at the N-terminus (E39V, M47A, R76A) (Fig. S3 and S4). Using these two constructs, K_i of the mLptA-LptAm interaction was determined by fluorescence polarization (FP) as 34.9 ± 3.0 nM.

To probe the LptA-LptC interaction, we modified a previously described periplasmic LptC construct[21] at two sites (Y60A, R61A) to yield a monomeric construct[22], LptC^{AA} (Fig. S3). The well-defined heterodimer LptAm-LptC^{AA} is characterized by a K_i of 1.8 ± 0.4 μM. (Fig. S5). NMR and SEC-MALS data reveal formation of the respective dimer via the suspected interface (Fig. S5 and S22). The K_i values for corresponding interactions of the thanatin-resistant mutant LptAm^{Q62L} with mLptA and LptC^{AA} were 69.0 ± 14.8 nM and 26.7 ± 3.5 μM, respectively. Similar values were determined for the *K. pneumoniae* proteins. See Tab. S11 for further information.

*Disassembly of the periplasmic bridge by compound **4***

Next, we used size-exclusion chromatography (SEC) and NMR to probe the integrity of protein-protein interactions upon addition of **4**. The SEC chromatogram reveals that peaks from the dimeric species disappear and two new peaks from the monomers arise when **4** is added to the protein mixture (Fig. 5B). We complemented the SEC studies

by [^{15}N,^{1}H]-HSQC NMR experiments. Two sets of experiments were measured for each protein-protein pair, in which one of the two interacting proteins was uniformly ^{15}N labeled while the cognate partner was unlabeled and vice versa. Representative NMR spectra and SEC traces in Fig. 5C demonstrate that both the LptAm-mLptA and the LptAm-LptC^{AA} interactions were completely disrupted by **4** in agreement with previous reports[17]. Upon addition of **4**, signals from LptAm-mLptA and LptAm-LptC^{AA} perfectly superimpose with those from LptAm-**4**, mLptA-**4** or LptC^{AA}. The K_i for the LptAm-**4** interaction of 1.9 ± 0.1 nM is 18 times stronger than the LptAm-mLptA interaction (K_i = 34.9 ± 3.0 nM). While thanatin binds to LptAm^{Q62L} with a K_i of 38.9 ± 7.9 nM - and approximates within the 95% CI of the mLptA-LptAm^{Q62L} interaction (K_i = 64.0 ± 21.8 nM) - in contrast, **4** and **5** bind with higher affinities of 16.1 ± 3.4 and 22.5 ± 6.1 nM, respectively. In agreement, SEC chromatograms reveal that thanatin fails to completely disassemble the LptAm^{Q62L}-mLptA complex (Fig. S21), while compound **4** achieves almost complete disassembly.

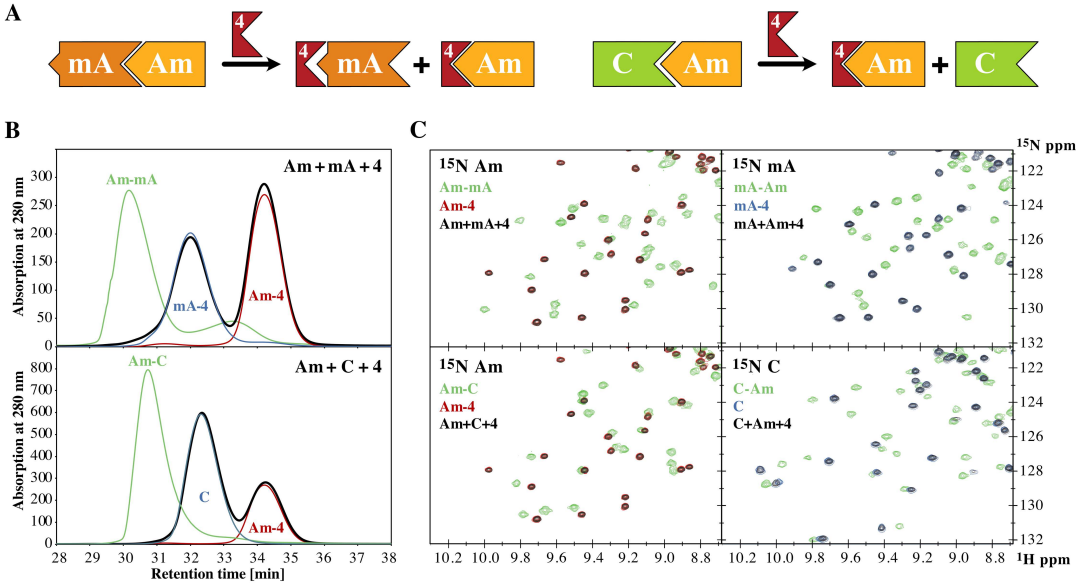

Fig. 5: Disassembly of *E. coli* dimers. **A** Schematic overview of the disassembly process. Abbreviations are used for Lpt proteins (A=LptA, C=LptC^{AA}). **B** SEC trace from the mLptA-LptAm (top) and LptAm-LptC^{AA} (bottom) mixtures in presence of **4** (bold black lines). SEC traces of the protein dimers (green lines) or from the **4** complexes with LptAm, mLptA or with LptC^{AA} are shown (thin blue and red lines). **C** [^{15}N,^{1}H]-HSQC spectra from the mLptA-LptAm (top) and LptAm-LptC^{AA} (bottom) mixtures in presence of **4**. In presence of **4**, the peaks of mixtures of the dimeric proteins superimpose with those of the corresponding monomeric proteins. In both NMR and SEC experiments the protein concentration was 200 µM and 1.5 equiv. of peptide were added. For a complete set of all SEC or NMR data see Fig. S21.

Discussion

Thanatin's promising antimicrobial spectrum and intriguing non-membranolytic mode of action inspired us to develop a novel class of antibiotics. The resulting peptide **4** show potent antimicrobial activity in mouse lung and thigh infection models, drug-like ADME and PK properties and no safety findings in a 7-day mouse study with q12h dosing up to 30 mg/kg/day. Appropriately N- or C-terminally modified LptA or LptC proteins used in biophysical and structural biology studies permitted the investigation of individual interactions in the periplasmic Lpt protein bridge. These studies revealed that the mode-of-action of the peptides is the competitive disruption of LptA-LptA and the LptA-LptC interactions.

The thanatin peptide scaffold, which is large compared to classical small molecule antibiotics, allowed for on-target activity optimization of synthetic peptides. It resulted in analogs with higher affinity to both LptA and functional mutants of LptA, overcoming resistance. The prevalence of mutations in LptA, identified by whole genome sequencing of a large panel of thanatin-resistant bacterial mutants, and the low MIC values of **3**-**5** against these strains is consistent with the lower propensity of these novel compounds to select for resistant mutants. Accordingly, K_is of **4** or **5** to LptAm remained largely unchanged but dropped for binding to $LptAm^{Q62L}$. Importantly, increased compounds' binding affinities to $LptAm^{Q62L}$ corresponded to reduced resistance frequencies when compared to thanatin. While the binding constants of our peptides to LptAm generally correlated with MIC values, there were still exceptions, indicating that additional factors were optimized for these compounds like membrane permeation, periplasmic stability, or binding to LptD[19].

The antibacterial activity spectrum of our macrocyclic peptides is related to LptA sequence conservation in the corresponding bacteria relative to *E. coli*. The thanatin analogs are active against MDR and XDR Enterobacteriaceae strains expressing carbapenemases and/or other resistance determinants, and address key WHO priority 1 AMR Gram-negative bacteria. Preliminary experiments demonstrated that **4** binds with reduced affinity to LptAm from phylogenetically distant bacteria suggesting that the optimization of this scaffold against other ESKAPE pathogens would be possible. The observed potent activity of **4** in mouse models of lung and thigh infections warrants further preclinical and potentially clinical studies.

Material and methods

Cloning, expression and purification of proteins

To increase stability and solubility all proteins were expressed as C-terminal fusions to the highly soluble 62-residue protein G from *Streptoccocus sp.* (GB1)[23]. Proteins of interest were released by cleavage with the TEV protease leaving only an N-terminal glycine as an additional amino acid. For exact sequences see Tab. S2.

The monomeric N-terminal truncated LptA version (LptAm) was previously used in Vetterli *et al*[16]. The resistant mutant $LptAm^{Q62L}$ contained only the Q62L mutation when compared to LptAm. The mutant mLptA was designed to avoid formation of dimer contacts with LptA at its N-terminus. During the design, a model of the dimer was made, based on PDB entry 2R19, and an alanine screen was performed using the program package MOE to obtain residue-specific ΔStability and ΔAffinity values. The best hits (high affinity change and low stability change) were expressed, and the $LptA_{25-185}$ mutant E39V M47A R76A was selected as the best candidate. LptC Y60A R61A ($LptC^{AA}$) comprises only the periplasmic domain of $LptC_{25-191}$ (truncated after the transmembrane helix). The previously described double mutation Y60A and R61A was introduced to avoid head-to-head dimerization[22]. All mutations and truncations of the *E. coli* constructs could be transferred to the *K. pneumoniae* sequences due to their high sequence homology. The corresponding *K. pneumoniae* proteins were purified with similar yields and displayed similar properties.

All proteins were expressed in *E. coli* BL21 (DE3) cells at 25°C in M9 media prepared according to Schuster *et al*.[24] following induction with 0.5 mM IPTG at an OD_{600} of 0.6–1.0.

Cells were lysed and the fusion proteins extracted by Ni-NTA affinity chromatography. The His_6-GB1 tag was removed with the TEV protease, followed by a reverse Ni-NTA step to remove the fusion partner. The yields of the expressed Lpt proteins were between 15–60 mg/L of M9 expression medium. Purified proteins were characterized by SDS-PAGE, SEC-MALS and MS (Fig. S1-5). The final concentration for the NMR samples were 200-600 µM, in 20 mM Na-Pi pH 7, 150 mM NaCl and 10% D_2O.

Peptide synthesis

Thanatin and peptides **2-5** were synthesized by solid phase peptide synthesis (SPPS) using the Fmoc/tBu strategy[25]. The peptide was assembled by standard automated Fmoc SPPS on 0.025 mmol scale (based on pre-loaded resin loading). To introduce the

guanidine (Gua) group in **5**, after final Fmoc removal, the peptide resin was treated with N,N'-bis-Boc-1-guanylpyrazole. After simultaneous peptide release from the resin and global side chain deprotection with a trifluoroacetic acid-based cocktail, the disulfide bridge was formed by oxidation with DMSO. The crude cyclic product was purified by reversed phase HPLC. To introduce the fluorophore in **4**-FL**,** the peptide precursor bearing the 6-azido-L-lysine to replace K17' (Fig. S6) was synthesized. The purified peptide was then coupled to Alexa Fluor 647 alkyne by copper-catalyzed azide-alkyne cycloaddition. For more details on the synthetic procedures and full analytical characterization of the peptides, see the SI.

Biological profiling of the compounds

To access the pharmacological profile, the haemolytic behaviour, cytotoxicity, plasma stability and plasma protein binding were measured. All data were determined in biological replicates.

To test their haemolytic potential, compounds were incubated in the presence of phosphate-buffered-saline (PBS)-washed human red blood cells. After 1 h incubation at 200 mg/L and 37°C, the samples were centrifuged (3220 g), and the supernatants diluted in Dulbecco's PBS (DPBS) and optical density at 540 nm determined (OD_{540})). The haemolysis induced by the compound was calculated versus a 100% lysis control prepared with 2.5% Triton X-100 (Tab. S4A).

The cytotoxicity of compounds was determined by determining the number of viable cells using the Sigma Cell Counting Kit-8 (WST-8). Hela cells were incubated at 37°C and 5% CO_2 for 24 h, after which the medium was replaced with fresh medium containing dilutions of compounds. After another 48h, cell viability was monitored by addition of WST-8 solution and measurement of optical density at 450 nm (OD_{450}) (Tab. S4A).

To determine plasma stability, compounds were incubated for 0, 15, 30, 60, 120 and 240 min in K3EDTA-stabilized plasma of human and CD-1 mice (BioIVT). Samples were extracted by precipitation with 3 volumes of acetonitrile +0.5% TFA, and their stability was determined by LC–MS/MS (Tab. S4A).

Plasma protein binding was determined by the mass balance method using a 30-kDa cut-off filter to separate free from plasma-protein bound compounds in pooled human and mouse plasma samples. The compounds were diluted in pH 7.5-adjusted plasma to a final concentration of 10 mg/L and incubated for 30 min at 37°C. After ultrafiltration,

protein binding was determined by subtracting the percentage of compound in ultrafiltrate from the total amount of compound in spiked plasma (Tab. S4A).

In vivo tolerability studies and pharmacokinetic analysis

To set a dose for the PK and *in vivo* efficacy studies that does not produce mortality or overt clinical signs of toxicity the 'Autonomic Signs' study design was applied. Test substances were administered intravenously to a group of three male ICR mice (CD-1 mice), which were monitored for acute toxic symptoms and autonomic effects at 30, 60, 120, 180 and 240 min after first administration. The mice were then observed again for mortality up to 7 days after compound administration (Tab. S4B).

PK were studied in adult CD-1 male mice following either a single dose of 10 mg/kg subcutaneous (SC) injection or by a single dose of 5 mg/kg IV (bolus) injection to the tail vein. Plasma samples were taken from 9 mice in each treatment group at 0.25, 0.5, 1, 2, 3, 4, 8 h post-dose (for single SC administration) or at 0.083, 1, 2, 4, 8, 12 h post-dose (for single IV administration). Blood samples (in Li-heparin as anticoagulant) were collected from the retrobulbar venous plexus under short isoflurane anaesthesia. Plasma samples were obtained by centrifugation for 10 min at 3'000 g and 4°C and the supernatant analysed by LC-MS/MS. After separation on a phenyl-hexyl reverse phase column using an acetonitrile-water gradient, peaks were analysed by ESI-MS. The mean plasma concentration and the standard deviation from all three mice within each time point were calculated, and PK parameters of test agent were calculated with a non-compartmental analysis model based on WinNonlin, using a trapezoid area calculation (Tab. S4B).

Mouse models of peritonitis, lung and thigh infections

To evaluate the *in vivo* efficacy of peptide **4** to treat peritoneal infections, adult immunocompetent female ICR mice (8 per group) were infected on day 0 by intraperitoneal (IP) administration of 1.54×10^5 CFU/ml *E. coli ATCC 25922* with 5% mucin into the peritoneum. The vehicle saline was administered IV BID q12h at 1 and 13 h after infection. The peptide **4** was IV administered twice (BID) at 1 and 13 h post-infection (q12h) at 15 and 30 mg/kg/day. Control reference agent, Levofloxacin at 1 mg/kg was administered SC QD at 1 h post infection. The animals were monitored for survival up to 7 days, twice daily. The significance of the survival rate was assessed with the Fisher's exact test (Fig. S7A).

To evaluate the *in vivo* efficacy of peptide **4** to treat thigh infections, male CD-1 mice (6 per group) were rendered neutropenic with IP injections with cyclophosphamide on day -4 (150 mg/kg) and day -1 (100 mg/kg). Mice were infected 24 hours post the second dose of immunosuppressive agent by intramuscular instillation with *E. coli* ATCC 25922 diluted to an optimal concentration with PBS. For infection mice were temporarily anaesthetized using inhaled isoflurane (2.5% isoflurane / 97.5% oxygen). Anaesthetised mice were infected with 0.05mL inoculum by intramuscular instillation into each lateral thigh muscle. The inoculum concentration was 3.03×10^6 cfu/mL (1.52×10^5 cfu/thigh). The peptide **4**, was administered IV at a total dose level of 30 mg/kg/day fractionated q4h, q6h and q12h equating to individual doses of 5, 7.5 and 15 mg/kg, respectively. Control reference agent, Polymyxin B, was administered SC at a total dose level of 40 mg/kg/day q12h, at 2 and 14 h after infection. Additional groups were included that were euthanized pre-treatment (2 h after infection) or treated with vehicle (IV 0.9% saline BID q12h at 2 and 14 h after infection) only. At 26 h post-infection, the clinical condition of all mice was assessed, the mice euthanized by pentobarbitone overdose and thigh tissue harvested, weighed, and homogenized. Thigh-sample homogenates were quantitatively cultured onto agar for determination of the counts of CFU per thigh (Fig. S7B). Data from the efficacy study was analysed using StatsDirect software (version 3.1.8). The non-parametric Kruskal-Wallis test was used to test all pairwise comparisons (Conover-Inman) for tissue burden data. For the purposes of this study, each thigh was considered an independent infection site, generating two data points per mouse.

To evaluate the *in vivo* efficacy of peptide **4** to treat lung infections against *K. pneumoniae* AR-BANK #0160, female ICR mice (5 per group) were rendered neutropenic with IP injections with cyclophosphamide on day -4 (150 mg/kg) and day -1 (100 mg/kg). Mice were infected 24 h after the second dose of immunosuppressive agent by intranasal injection of *K. pneumoniae* AR-BANK #0160 inocula with a total volume of 20, 10 µL per nostril (1.02×10^6 CFU/mL). The peptide **4** was administered IV BID q12h, at 2 and 14 h after infection, at 0.5, 1, 2, 4, 8, 15 and 30 mg/kg/day. Control reference agent, Levofloxacin at 40 mg/kg/day was administered SC BID q12h, at 2 and 14 h after infection. Additional groups were included that were euthanized pre-treatment (2 h after infection) or treated with vehicle (IV 0.9% saline BID q12h at 2 and 14 h after infection) only. At 26 h post-infection, the clinical condition of all mice was assessed, the mice euthanized by CO_2 asphyxiation and lung tissue harvested,

weighed, and homogenized. Pathogen burden was enumerated with the serial dilution plating technique. The colony forming unit value per g tissue (CFU/g) was calculated and compared to a vehicle group (Fig. S7C). Significance of effects was assessed with one-way ANOVA followed by Dunnett's test.

To evaluate the *in vivo* efficacy of **4** to treat lung infections against *K. pneumoniae* ATCC 43816, male ICR mice (6 per group) were rendered neutropenic with injections with cyclophosphamide on day -4 (200 mg/kg) and day -1 (150 mg/kg). Mice were infected 24 h after the second dose of immunosuppressive agent by intranasal injection of *K. pneumoniae* ATCC 43816. For infection animals were anaesthetised with a ketamine (50 mg/kg) and medetomidine (0.5 mg/kg) anaesthetic cocktail via IP injection (10 mL/kg). Anaesthetised mice were infected with 0.04 mL inoculum by intranasal instillation into mouse nostrils (20µL per nostril, 5 min between nostrils). The inoculum concentration was $1.97x10^6$ cfu/mL ($7.87x10^4$ cfu/mouse). Once the procedure had been completed the anaesthetic reversal agent atipamezole was administered at 3.75 mg/kg SC. The peptide **4** was administered IV BID q12h, at 2 and 14 h after infection at 05, 1, 2, 4, 8, 15 and 30 mg/kg/day. Control reference agent, Meropenem at 300 mg/kg/day was administered IV QID q6h, at 2, 8, 14 and 20 h after infection. Additional groups were included that were euthanized pre-treatment (2 h after infection) or treated with vehicle (IV 0.9% saline BID q12h at 2 and 14 h after infection) only. At 26 h post-infection, the clinical condition of all mice was assessed, the mice euthanized by by pentobarbitone overdose and lung tissue harvested, weighed, and homogenized. Pathogen burden was enumerated with the serial dilution plating technique. The colony forming unit value per g tissue (CFU/g) was calculated and compared to a vehicle group (Fig. S7D). Data from the efficacy study was analysed using StatsDirect software (version 3.1.8). The non-parametric Kruskal-Wallis test was used to test all pairwise comparisons (Conover-Inman) for tissue burden data.

Microbiology

MIC assays (CLSI methodology) and serial passage studies were performed as described by Luther *et al.*[6]. The spontaneous mutation frequencies of thanatin and analogues using reference strains of *E. coli* (ATCC 25922) and *K. pneumoniae* (ATCC 43816) were determined by inoculating agarose containing the compounds at concentrations 4-, 8- and 16-fold over the MIC. Resistant mutants were isolated, their

MIC values determined and sent to Microbes NG (Birmingham, UK) for whole genome sequencing and bioinformatic analysis.

Binding Assays

Binding affinities were determined by fluorescence polarization. All binding affinity assays were performed in triplicates and executed at ambient temperature (25°C) using freshly prepared protein stocks. Anisotropy was measured using the Tecan Safire^2 plate reader (Tecan Trading AG, Switzerland) using a 10 nm bandwidth and setting the excitation and emission wavelengths to 635 nm and 670 nm, respectively.

For direct binding assays, a fixed concentration of the fluorescently labeled peptide, **4**-FL, a derivative of **4**, was added to a serial dilution of the corresponding Lpt protein. For the indirect binding assays, a fixed concentration of protein and fluorescently labeled peptide were mixed in a 1:1 ratio, and subsequently added to a serial dilution of the unlabeled peptide. Data were fit to a sigmoidal interpolation model on GraphPad Prism 9 to generate IC_{50} values for each unlabeled peptide, and the corresponding inhibition constants (K_is) were calculated using the Cheng-Prusoff equation. For details see SI.

NMR spectroscopy, assignments and structure calculations

Backbone chemical shifts of **4**-bound *E. coli* LptAm, LptAm^{Q62L}, *K. pneumoniae* LptAm and of free LptC^{AA} were assigned using spectra obtained from a standard set of 3D triple-resonance experiments using ^{13}C,^{15}N-labeled proteins[26]. The protein-free peptide **4** was dissolved in acetate buffer, pH 4.0, and assigned using standard 2D homonuclear NOESY, COSY and TOCSY spectra. The structure of the free peptide was calculated from the 300 ms NOESY spectrum. To unambiguously distinguish the intermolecular from the intramolecular NOEs differently-labeled LptAm and thanatin were used in Vetterli *et al.*[16]. In the case of **4** this was not possible because the peptide contains unnatural amino acids. Therefore, ^{2}H,^{15}N-LptA grown in D_2O using perdeuterated glucose was used, in which the residual proton density was less than 1%. This sample in combination with **4** allowed to record 2D [^{1}H,^{1}H], ^{15}N-filtered, NOESY spectra[27] to obtain intra-ligand NOEs exclusively. Intermolecular sidechain NOEs were extracted from a ^{13}C-edited, ^{13}C filtered NOESY experiment. Upper-distance restraints were derived from 80 ms ^{15}N and 2 sets of ^{13}C-resolved 3D NOESY spectra, centered on aliphatic (39 ppm) and aromatic (120 ppm) carbons. NOESY spectra were iteratively automatically assigned using the CYANA macro *noeassign*[28]. Additional torsion angle

restraints were derived from backbone chemical shifts using the program TALOS+[29]. For more details of the structure calculations see Tab. S13.

All coordinates and chemical shifts of *E. coli* LptAm-**4**, *E. coli* LptAm^{Q62L}-**4** and *K. pneumoniae* LptAm-**4** were deposited to the PDB (BMRB) data bases under accession codes 7QS6 (34699), 7ZED (34720), and 7ZAX (34716), respectively.

Molecular dynamics simulations

MD simulations were conducted using the program package Gromacs 2020[30], that employs the CHARMM36-jul2020 force field[31]. Parameters for the non-natural amino acids (Gua-Val, Hyp, Dab, Pen) were inferred from the existing CHARMM force field. Initially, the NMR-derived starting structures were relaxed in a box of SPC water followed by a short dynamics run at constant volume and temperature (300K) for 100 ps using a 2 fs timestep. MD production runs had total lengths of 2 μs and integration steps of 2 fs. For more details of the MD calculations see the SI.

Acknowledgements

We acknowledge funding of this project by Innosuisse (grant No. 33285.1 IP-LS). We further thank Simon Jurt for help with the NMR spectroscopy; Dr. Katja Zerbe, Argton Zeqiri and Laetitia Rožić in the biochemical part; Christian Bauman, Jens Soebek and the Functional Genomics Center Zurich (FGCZ) for their help with the FP analysis and Dr. Fred Naider for critical reading.

Spexis AG (formerly Polyphor AG) acknowledge that the research reported in this publication is also supported by CARB-X. CARB-X funding for this project is sponsored by the Cooperative Agreement Number IDSEP160030 from ASPR/BARDA and by awards from Wellcome Trust and Germany's Federal Ministry of Education and Research (BMBF). The contents are solely the responsibility of the authors and do not necessarily represent the official views of CARB-X or any of its funders. In addition, Spexis AG (formerly Polyphor AG) has utilized the National Institute of Allergy and Infectious Diseases' suite of preclinical services for *in vivo* evaluations (Contract No. HHSN272201700020I 75N93020F00159 (A-42).

Author contributions

F.J, D.O. and O.Z. acquired funding for the project and oversaw execution of all aspects of the project.
M.B., E.B., D.O., M.S., K.K.O. and O.Z. wrote the manuscript with contributions from all other authors who also agreed to the final version.
A.L., G.U. and E.B. directed chemistry; H.L. and M.B. directed microbiology and design of studies; and A.W. directed drug metabolism and pharmacokinetics, efficacy, and toxicology studies.
E.B., N.D., K.L.P., S.H., S.G., V.R., P.Z., and G.U. performed medicinal chemistry experiments and evaluations.
C.L., S.S., and C.d.A. performed microbiological experiments, and evaluations.
S.D., T.R., and S.D.M performed ADMET, drug metabolism, and pharmacokinetics experiments and evaluations.
S.D.M and P.M. monitored *in vivo* efficacy and safety studies and evaluations.
M.S. designed and produced all protein constructs of the Lpt bridge, analyzed those data, and supervised the biochemical part.
K.K.O. produced all LptA proteins for which structures were determined, elucidated the structure of the *K. pneumoniae* LptAm complex and determined binding affinities by FP.
K.M. determined the structures of the *E. coli* LptAm and LptAm^{Q62L} complexes, conducted and analyzed MD simulations and oversaw the structure elucidation part.

All authors contributed to the analysis and interpretation of results.

Competing interests

E.B, N.D., K.L.P., S.H., S.G., V.R., S.D., P.Z., A.L., C.L., S.S., C.d.A., H.L., T.R., S.D.M, P.M., A.W., F.J., G.U., D.O. and M.B. declare competing interests as current or former employees of Spexis AG who pursue clinical studies.

References:

1 Antimicrobial Resistance, C. Global burden of bacterial antimicrobial resistance in 2019: a systematic analysis. *Lancet*, doi:10.1016/S0140-6736(21)02724-0 (2022).

2 Boucher, H. W. *et al.* Bad bugs, no drugs: no ESKAPE! An update from the Infectious Diseases Society of America. *Clin. Infect. Dis.* **48**, 1-12, doi:10.1086/595011 (2009).

3 Tacconelli, E. *et al.* Discovery, research, and development of new antibiotics: the WHO priority list of antibiotic-resistant bacteria and tuberculosis. *Lancet Infect. Dis.* **18**, 318-327, doi:10.1016/S1473-3099(17)30753-3 (2018).

4 Tzouvelekis, L. S., Markogiannakis, A., Piperaki, E., Souli, M. & Daikos, G. L. Treating infections caused by carbapenemase-producing Enterobacteriaceae. *Clin. Microbiol. Infect.* **20**, 862-872, doi:10.1111/1469-0691.12697 (2014).

5 Srinivas, N. *et al.* Peptidomimetic antibiotics target outer-membrane biogenesis in *Pseudomonas aeruginosa*. *Science* **327**, 1010-1013, doi:10.1126/science.1182749 (2010).

6 Luther, A. *et al.* Chimeric peptidomimetic antibiotics against Gram-negative bacteria. *Nature* **576**, 452-458, doi:10.1038/s41586-019-1665-6 (2019).

7 Imai, Y. *et al.* A new antibiotic selectively kills Gram-negative pathogens. *Nature* **576**, 459-464, doi:10.1038/s41586-019-1791-1 (2019).

8 Hart, E. M. *et al.* A small-molecule inhibitor of BamA impervious to efflux and the outer membrane permeability barrier. *Proc. Natl. Acad. Sci. U S A* **116**, 21748-21757, doi:10.1073/pnas.1912345116 (2019).

9 Sherman, D. J. *et al.* Lipopolysaccharide is transported to the cell surface by a membrane-to-membrane protein bridge. *Science* **359**, 798-801, doi:10.1126/science.aar1886 (2018).

10 Lundstedt, E., Kahne, D. & Ruiz, N. Assembly and Maintenance of Lipids at the Bacterial Outer Membrane. *Chem. Rev.* **121**, 5098-5123, doi:10.1021/acs.chemrev.0c00587 (2021).

11 Sperandeo, P., Martorana, A. M. & Polissi, A. Lipopolysaccharide biogenesis and transport at the outer membrane of Gram-negative bacteria. *Biochim. Biophys. Acta Mol. Cell. Biol. Lipids* **1862**, 1451-1460, doi:10.1016/j.bbalip.2016.10.006 (2017).

12 Mahalakshmi, S., Sunayana, M. R., SaiSree, L. & Reddy, M. yciM is an essential gene required for regulation of lipopolysaccharide synthesis in *Escherichia coli*. *Mol. Microbiol.* **91**, 145-157, doi:10.1111/mmi.12452 (2014).

13 Guest, R. L. *et al.* YejM Modulates Activity of the YciM/FtsH Protease Complex To Prevent Lethal Accumulation of Lipopolysaccharide. *mBio* **11**, e00598-00520, doi:doi:10.1128/mBio.00598-20 (2020).

14 Clairfeuille, T. *et al.* Structure of the essential inner membrane lipopolysaccharide–PbgA complex. *Nature* **584**, 479-483, doi:10.1038/s41586-020-2597-x (2020).

15 Sperandeo, P. *et al.* Functional analysis of the protein machinery required for transport of lipopolysaccharide to the outer membrane of *Escherichia coli*. *J. Bacteriol.* **190**, 4460-4469, doi:10.1128/JB.00270-08 (2008).
16 Vetterli, S. *et al.* Thanatin targets the intermembrane protein complex required for lipopolysaccharide transport in *Escherichia coli*. *Sci. Adv.* **4**, eaau2634, doi:10.1126/sciadv.aau2634 (2018).
17 Moura, E. C. C. M. *et al.* Thanatin Impairs Lipopolysaccharide Transport Complex Assembly by Targeting LptC–LptA Interaction and Decreasing LptA Stability. *Front. Microbiol.* **11**, doi:10.3389/fmicb.2020.00909 (2020).
18 Fehlbaum, P. *et al.* Structure-activity analysis of thanatin, a 21-residue inducible insect defense peptide with sequence homology to frog skin antimicrobial peptides. *Proc. Natl. Acad. Sci. U S A* **93**, 1221-1225, doi:10.1073/pnas.93.3.1221 (1996).
19 Fiorentino, F. *et al.* Dynamics of an LPS translocon induced by substrate and an antimicrobial peptide. *Nat. Chem. Biol.* **17**, 187-195, doi:10.1038/s41589-020-00694-2 (2021).
20 Laguri, C. *et al.* Interaction of lipopolysaccharides at intermolecular sites of the periplasmic Lpt transport assembly. *Sci. Rep.* **7**, 9715, doi:10.1038/s41598-017-10136-0 (2017).
21 Schultz, K. M. & Klug, C. S. Characterization of and lipopolysaccharide binding to the *E. coli* LptC protein dimer. *Protein Sci.* **27**, 381-389, doi:10.1002/pro.3322 (2018).
22 Schultz, K. M., Fischer, M. A., Noey, E. L. & Klug, C. S. Disruption of the *E. coli* LptC dimerization interface and characterization of lipopolysaccharide and LptA binding to monomeric LptC. *Protein Sci.* **27**, 1407-1417, doi:10.1002/pro.3429 (2018).
23 Zhou, P., Lugovskoy, A. A. & Wagner, G. A solubility-enhancement tag (SET) for NMR studies of poorly behaving proteins. *J. Biomol. NMR* **20**, 11-14 (2001).
24 Schuster, M. *et al.* Optimizing the α_{1B}-adrenergic receptor for solution NMR studies. *Biochim. Biophys. Acta Biomembr.* **1862**, 183354, doi:10.1016/j.bbamem.2020.183354 (2020).
25 Behrendt, R., White, P. & Offer, J. Advances in Fmoc solid-phase peptide synthesis. *J. Pept. Sci.* **22**, 4-27, doi:10.1002/psc.2836 (2016).
26 Sattler, M., Schleucher, J. & Griesinger, C. Heteronuclear multidimensional NMR experiments for the structure determination of proteins in solution employing pulsed field gradients. *Prog. Nucl. Magn. Reson. Spectrosc.* **34**, 93-158 (1999).
27 Otting, G. & Wüthrich, K. Heteronuclear filters in two-dimensional (^{1}H,^{1}H) NMR spectroscopy: combined use with isotope labelling for studies of macromolecular conformation and intermolecular interactions. *Q. Rev. Biophys.* **23**, 39-96 (1990).
28 Güntert, P. Automated NMR structure calculation with CYANA. *Methods Mol. Biol.* **278**, 353-378 (2004).
29 Shen, Y. & Bax, A. Protein backbone and sidechain torsion angles predicted from NMR chemical shifts using artificial neural networks. *J. Biomol. NMR* **56**, 227-241, doi:10.1007/s10858-013-9741-y (2013).
30 Bekker, H. *et al.* Gromacs - a Parallel Computer for Molecular-Dynamics Simulations. *Physics Computing '92*, 252-256 (1993).
31 Best, R. B. *et al.* Optimization of the Additive CHARMM All-Atom Protein Force Field Targeting Improved Sampling of the Backbone phi, psi and Side-Chain chi(1) and chi(2) Dihedral Angles. *J. Chem. Theo. Comput.* **8**, 3257-3273, doi:10.1021/ct300400x (2012).

Supplementary Files

This is a list of supplementary files associated with this preprint. Click to download.

- SupplementaryMaterials010422final.pdf